Analysis of the effects of dimples on the performance of Small-Scale Horizontal Axis Wind Turbines with CFD

Imam Muzaki[a]*, Ismail Ismail[b]
[a]Department of Mechanical Engineering, Muhammadiyah Tegal University
kalibakung. Tegal, Jawa Tengah 52464, Indonesia
[b]Department of Mechanical Engineering, Pancasila University
Srengseng Sawah. Jagakarsa, DKI Jakarta, 12640, Indonesia
*E-mail: imammuzaki4bulan@gmail.com

Abstract (10pt Bold)

The addition of dimples to small-scale wind turbine blades can improve the energy extraction of horizontal axis wind turbines (HAWTs). However, although there is some understanding of how dimples affect wind turbine power, the effects of specific wind turbine blade stress parameters remain to be investigated. This article describes the impact of adding dimples to small-scale horizontal axis wind turbine (SSHAWT) blades. The results showed that the addition of dimples to SSHAWT 3, revealed that the addition of dimples with 27 dimples resulted in the highest turbine power, compared to the baseline wind turbine blade, with an average turbine output power of 362.25 w, at a wind speed of 6 m/s. The addition of dimples to wind turbine blades can be a suggestion for improving the performance of small-scale wind turbines.

Keywords: Efficiency; Fluid dynamic; Power; Torque.

Abstrak (10pt Bold)

Penambahan lesung pipit pada bilah turbin angin skala kecil dapat meningkatkan ekstraksi energi turbin angin sumbu horizontal (HAWT). Namun, meskipun ada beberapa pemahaman tentang bagaimana lesung pipit memengaruhi daya turbin angin, efek parameter tegangan bilah turbin angin tertentu masih harus diselidiki. Artikel ini menjelaskan dampak penambahan lesung pipit pada bilah turbin angin sumbu horizontal skala kecil (SSHAWT). Hasil penelitian menunjukkan bahwa penambahan lesung pipit pada SSHAWT 3, mengungkapkan bahwa penambahan lesung pipit dengan 27 lesung pipit menghasilkan daya turbin tertinggi, dibandingkan dengan bilah turbin angin dasar, dengan daya keluaran turbin rata-rata 362,25 w, pada kecepatan angin 6 m/s. Penambahan lesung pipit pada bilah turbin angin dapat menjadi saran untuk meningkatkan kinerja turbin angin skala kecil.

Kata kunci: Efisiensi; Dinamika fluida; daya; Torsi.

1. Introduction

There are many types of wind turbines, one of which is the horizontal axis (HAWT), which significantly affects how much electricity can be generated from wind energy with the highest degree of dependability and economy. [1] It promotes using creative and effective wind turbine systems in research [2], one of which is in small-scale wind turbine blades [3]. The HAWT generator directly converts the wind extracted from the rotor. The rotor blades can be rotated along their longitudinal axis to adjust the rotor speed and power output [4]. The potential of the HAWT model's small-scale wind turbine's aerodynamic performance on the SSHAWT indicates that during low-speed experiments, with a speed of 9 m / s producing a power of 470 w is an extraordinary achievement [5]. The greatest power value falls as the yaw angle increases at a wind speed. Significant improvements in blade performance are possible and require controllers and generators to be changed so the wind turbine does not experience jamming [6]. The small-scale wind turbine can achieve a power coefficient (Cp) of 0.255 with a specific wind speed of 6 m/s and a turbine height of 8.22 metres [7]

Several factors regarding wind turbine blade design optimization include manufacturing feasibility, cost, dependability, structural integrity, and aerodynamic effectiveness. There are two design optimization issues with wind turbine blades: optimization of structural and aerodynamic design [8]. Numerous studies have concentrated on just one aspect of the design, such as the optimization of aerodynamic design [9], [10] or structural design optimization [11], [12]. Design optimization in geometry, among other things, on airfoils [13], winglets [14], [15]. Wind turbine blades oriented horizontally were the subject of these investigations. Wind turbine blade optimization has been greatly enhanced recently. A growing number of wind turbine blades have dimples added for optimization. In addition to

increasing turbulence, adding dimples to the wind turbine blade's surface can lower its drag coefficient and raise its lift coefficient [16].

Applying dimples can be deemed essential as the impact is closely linked to the airfoil's angle of attack. Wind turbine blades of this type, V47-660 kW [17], demonstrate that dimples can efficiently boost torque and power generation when appropriately constructed. Dimples were added to the GEO 239 airfoil to enhance powder, adding dimples to the wind turbine blade's surface [18]. Wind turbines with two blades, namely the rotor NREL phase VI type, try adding dimples to the S809 airfoil. With the addition of dimples, Rotor blades produce better torque when approaching the end of the blade due to a reduction in the pressure coefficient, resulting in increased pressure [19]. This dimple is added based on golf balls with an uneven texture or dimples on the surface. Golf balls with uneven textures have a further trajectory after being hit. Bearman first proved scientific research in 1973 [20]. It is scientifically proven that golf balls with the addition of dimples on the surface have a smaller aerodynamic drag coefficient than golf balls with a flat surface. Recent research by Beratlis et al. [21]. This indicates that adding dimples also reduces the Reynolds Number, indicating that the substance's layer that borders with the addition of dimples becomes more turbulent than without dimples. In the latter part of this decade, research on SSHAWTs has increased. Small-scale wind turbines can be built in areas where wind speeds are not high enough to generate electricity, with wind speeds of 5 to 30 m/s [22]. Similarly, Reynold Number is assumed to be small-scale wind turbines, usually between 100000 and 4000000 [23]. High-strength materials will modify the blade of a small-scale wind turbine to boost efficiency [24]. It is exciting to modify the wind turbine blade with the addition of dimples because it has potential. SSHAWT has identical performance in areas with low wind speed and not too high-power output, with the addition of dimples making the power output higher than not using dimples on wind turbine blades. Assessments must be conducted, including the material's resistance to adding dimples to the wind turbine blades. Because the inclusion of dimples automatically reduces portions of the blade. It will be challenging in the real world to be accurate., let alone quickly, without proper computers and analysis software.

Along with the many studies related to adding dimples to the workpiece, especially on wind turbine blades, assessments of dimples need to be massively carried out. Adding dimples is a significant factor in improving performance on wind turbine blades because the power and torque become higher with dimples. The comprehensive novelty of this study is that it combines several studies that have been successful using the addition of dimples to large-scale horizontal wind turbine blades. Existing research the novelty of this research is to try to make an innovation on a small-scale horizontal wind turbine blade. Existing studies, such as the research conducted by Xie et al. [25], have successfully examined better heat transfer around the wind turbine blade with the addition of dimples than without dimples. Sedighi et al. [17] have also successfully researched the effect of adding dimples that can increase torque for a power plant. Research by Azlan et al. [19] has successfully explained the results of adding dimples, i.e., increased operating performance and good torque. This is due to increased pressure difference across the blades

Consideration of the design and application of the system is the initial capital to get wind potential first. The findings from earlier studies on adding dimples to the vacuum side of wind turbine blades of type V47-660 kW passively employed multiple dimples of radius positioned at various chord lengths and a particular separation from the hub. This study separated the dimples on the wind turbine blades into three variations. It used CFD simulations to maximize the evolving the small-scale horizontally axis wind turbine blades. Presenting performance results in the form of torque and power and velocity and pressure distribution using CFD simulations. The optimized blades are then implemented in low-speed wind turbines to validate the approach further and signal its potential application in the seismic assessment of wind turbines.

2. *Materials and Methods*

2.1. Dimple's parameter and blade dimension

The basic design for dimples in small-scale wind turbines was taken according to Suresh [26], which is suitable for application in rural areas. The wind speed of the wind turbine is limited from 2 m/s, 3 m/s, 4 m/s, 5 m/s to 6 m/s, which can be maximized for the SSHAWT. Fig. 1a presents the detailed shape and dimension of the proposed blade in this work. The dimples in the airfoil at the suction part regarding the wind direction. The present work uses three different variations for the dimples, as seen in Fig. 1b, with the detailed specification in Table 1.

Table 1. Turbine blade addition of dimple specifications

	BASE	SSHAWT 1	SSHAWT 2	SSHAWT 3
Location dimples (section)	-	2-4	2-7	2-9
Number of dimples (n)	-	9	18	27
Radius dimples (*r*) [mm]	-	5	5	5
Depth of dimples (*h*) [mm]	-	3	3	3
Wind speed (V) [m/s]	2,3,4,5,6	2,3,4,5,6	2,3,4,5,6	2,3,4,5,6
Distance of dimples (*s*) [mm]	-	20	20	20

The base blade used an airfoil type SD7080 with specifications from[27]. The SD7080 was taken as the base blade since it has many advantages for SSHAWT in low windspeed regions. Suresh evaluated the chord distribution for the

blade using wind speed [28].This speed is usually observed in areas with low wind speeds, so 2 m/s to 6 m/s was used as the wind speed in this study. The proposed model is suitable for simulating wind turbine operation in low-windspeed regions.

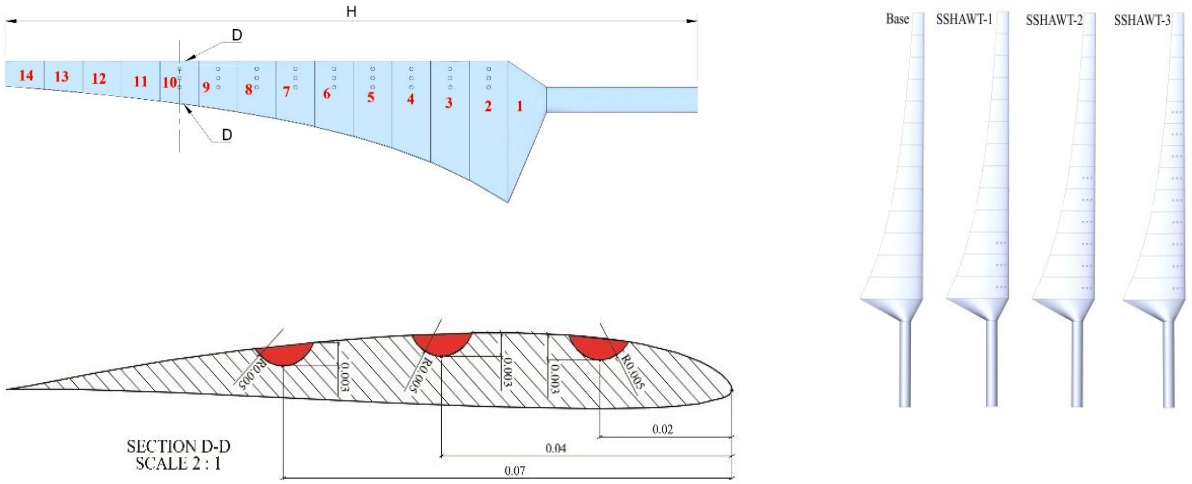

(a) **(b)**

Fig 1. Small-sacle horizontal axis wind turbine schematic: a) dimples profile and blade dimension, and b) variation of SSHAWT with three different dimple locations

2.2. Fluid Modelling

The proposed wind turbine blade was depicted using Ansys Fluent Sofware as a CFD [29]. Computational domain and boundary condition simulated airflow distribution for the proposed SSHAWT with dimples. It was modelled on the fluid domain (negative) of the system. The data for each SSHAWT model was obtained from this work. The profile of dimple variations is shown in Fig. 1.

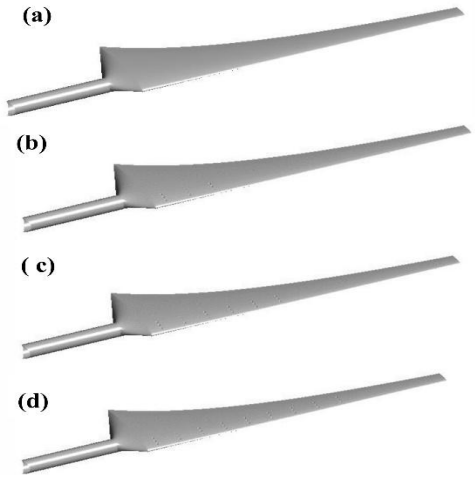

Fig 2. The geometry of the proposed turbine profile with dimple variation

Each blade's surface was defined according to its function (Fig 33). Meshing in CFD translates continuous fluid domains into separated computational domains that can be used to solve fluid equations numerically. The tetrahedron meshing method was used in this simulation because it can capture complicated shapes. The final meshing of the turbine part is shown in 3.

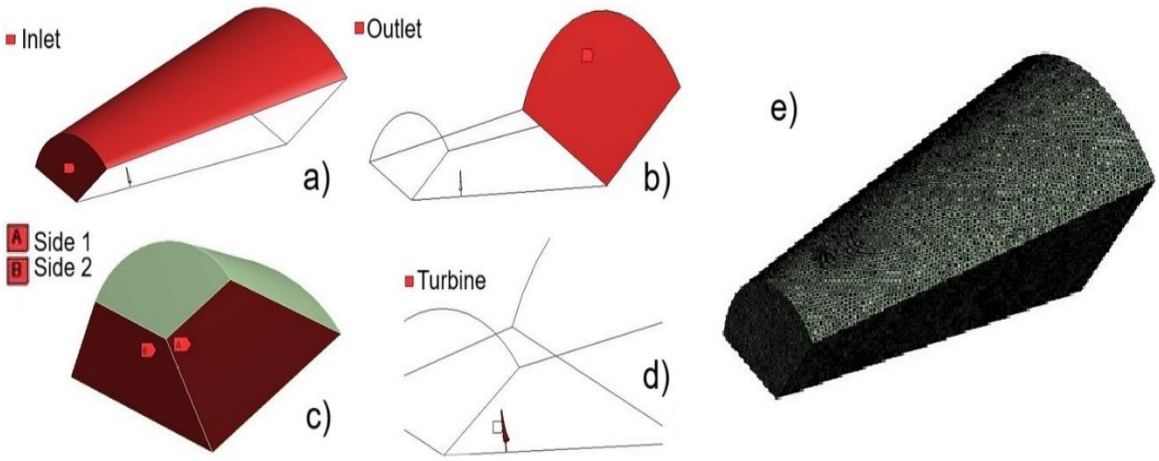

Fig 3. Turbine boundary: a) inlet location, b) outlet location, c) side location (periodic), (d) location; and e) meshing result

In turbulent flow studies, the Shear Stress Transport (SST) k-ω turbulence model is one of the approaches used to predict flow behavior under various conditions. This model combines two major turbulence models, namely the k-ω model developed by Wilcox and the k-ε model, in a hybrid computational method. This combination is intended to utilize the strengths of each model in handling various characteristics of turbulent flow. Wilcox's k-ω model predicts the flow near the wall, where the flow becomes more complex and requires high precision. On the other hand, the k-ε model is more effective in modeling free flow farther from the boundary surface. The mixing function automatically activates the k-ε model in the free flow area and the k-ω model near the wall to ensure a smooth transition between the two models. This approach improves the accuracy of turbulent flow simulations across a variety of geometries and flow conditions. [14]. The k-ω model simulates flow near sublayers, whereas the k-ε model predicts flow behaviour away from barriers [30]. As a result, it was concluded that the most effective for predicting airflow over wind turbines is the SST k-ω turbulence model, as shown in equations (1) and (2).

$$\frac{\partial}{\partial t}(\rho k) + \frac{\partial}{\partial xi}(\rho k u_i) = \frac{\partial}{(\partial kj}\left[\Gamma_k \frac{\partial k}{\partial kj}\right] + G_k - Y_k + s_k \quad (1)$$

$$\frac{\partial}{\partial t}(\rho\omega) + \frac{\partial}{\partial x_j}\left(\rho\omega u_j\right) = \frac{\partial}{\partial x_j}\left[\Gamma_\omega \frac{\partial \omega}{\partial x_j}\right] + G_\omega - Y_\omega + D_\omega + S_\omega \quad (2)$$

With Gk = min (Gk, 10ρβ* kω), S is the stress rate quantity of the flow inside the tunnel, the kinetic dissipation of turbulent kinetic energy k is Yk = ρβ* kω [35].

Cell zone condition for the fluid domain was given frame motion to represent rotation on the turbine with an angular speed of 15.5 rad/s. 2 m/s, 3 m/s, 4 m/s, 5 m/s and 6 m/s is the input for the boundary conditions at the inlet. The turbine surface is a wall non-slip condition representing attrition between the fluid and the wall. On the boundary side were periodic arrangements representing the turbine's three blades. A pressure outlet is necessary to present a flow outlet. The starting point for the iteration process was solution initialization. The nearer initial reference was expected as the expected solution. It was aimed at achieving a stable iteration process. As a result, it leads to smooth convergent conditions. The method was the standard initiation since it has one fluid direction from the inlet. The initial value was adjusted using default settings to the inlet and uncredited settings. Two criteria were used for the convergence of CFD analysis: Net Mass imbalance and residual values. It is possible to evaluate the convergence of CFD solutions using residual values. Six residual value variables are used in this work: continuity, kinetic turbulence (k), velocity (z), and specific rate of dissipation (ω), speed (x,y), specific rate of dissipation (ω) (k), which appeared throughout the computation process. The solution is possible when this residual value is less than 10^4 [31]. The net mass imbalance confirms further convergence, which should be less than 0.1% [32].

The fluid flow problem was a non-linear phenomenon, which made repetition during CFD analysis mandatory. The present work used iteration up to 1500 to ensure sufficient results from the CFD modelling. In addition, the standard initialization method was used, in which the initial value was calculated from the entry limit. Once the solution is converged, the blade's torque, pressure, and velocity can be plotted.

The output of the CFD refinement must be unaffected by the density and mesh size. Any reliance on it could indicate that the underlying flow physics has not been well examined. Thus, sensitivity tests and convergence simulations must be carried out to guarantee the mesh independence of the CFD findings. Table 2 displays four examples of different sizes that were created in order to look into grid independence. The study aims to assess grids 1 and 4, representing the coarsest and finest grids, respectively. Laminar boundaries between 0 to 5 and 5 to 30 are the sublayers and layers used, with y+ as the defining value. Maintaining a y+ value below one on a mesh of acceptable quality is necessary. The y+ value can be accurately determined using equation 3.

$$y^+ = \frac{\rho_w y u_\tau}{\mu_w} \tag{3}$$

All metrics in this state are within the acceptable range. In addition, a wide range of meshes were found after our analysis. Therefore, the values of Cd and Cp are not different. Therefore, it can be deduced that the CFD solution is unaffected by variations in the density and size of the mesh.

The calculated values of Cp and FD for various grids demonstrate consistency within a specific range. This consistency enhances the reliability of the findings. After comparing the grid values, we can determine that the cp value is less than 2% and the fd value is also less than 1% with this data, so it is included in the criteria for the data collection on grid 2. The results indicate that Grid 2 was an excellent choice for the CFD simulation.

Table 2. Summary of Grid Independence

Grid Features	First Grid	Second Grid	Third Grid	Fourth Grid
FD	13.68	13.61	13.57	13.46
Mesh element size (mm)	0.52	0.42	0.32	0.22
Number of elements X 10^3	85	109	153	230
Number of layers grow rate	1.17	1.15	1.13	1.11
C_p	0.45	0.49	0.38	0.43
Maximum Skewness	0.733	0.731	0.877	0.959
Number of layers	10	12	14	16
Averaged y+	1.6	1.1	1.03	0.94

Temporal and spatial discretization is necessary because of the irregular and unpredictable flow behaviour and the significant velocity gradient produced. An examination of temporal analysis is essential for precisely representing complex events. Ensuring the accuracy of CFD results requires the application of precise discretization methods in both temporal and spatial dimensions. In addition, to find out whether the amount of time used is appropriate for the numerical results, we need to use CFL as a validation. Because CFL is the key to knowing the best time, using equation 4.

$$CFL = \frac{u \bullet \Delta t}{\Delta} \tag{4}$$

The time step associated with $\Delta\theta = 2^\circ$ ($\Delta t = 0.001$(s)) and $\Delta\theta = 1^\circ$ ($\Delta t = 0.0005$(s)) was chosen for the current CFD simulation because of the comparable Cm pattern and the closeness of averaged C_m.

Wind turbine performance and aerodynamics are obtained with URANS calculations, namely the Reynolds number because it is imperative to get these characteristics. [33]. The calculation of the Reynolds Number can be done using Equation 5.

$$Re = \frac{V_{rel} C}{v} \tag{5}$$

The relative wind speed, measured in meters per second (m/s), is one of the critical factors in this analysis. In addition, the chord length, measured in meters (m), describes the object's physical dimensions under study. Meanwhile, the kinematic viscosity of air at 20°C has a fixed value of about 1.511 x 10^{-5} square meters per second (m^2/s). The classification of wind turbines based on the wind speed or Reynolds number (Re) achieved during operation can be divided into several categories. Low-speed wind turbines have Reynolds number values less than 10^3, medium-speed turbines operate at 10^3 to 10^5, and high-speed turbines have Reynolds numbers more significant than 10^5 [22]. Analysis of the chord distribution in small wind turbines shows a chord range between 0.05 m and 0.5 m. This chord distribution is essential as it affects the aerodynamic efficiency and overall performance of the turbine, which can optimize the surrounding airflow. The range of Reynolds numbers typically considered for small-scale wind turbines is between 100,000 and 400,000. These values reflect the flow conditions, where higher Reynolds numbers indicate a more turbulent flow, which can impact the stability and efficiency of the energy generated [23].

Calculating the Cp and Cq are fundamental aspects of turbine efficiency analysis. In other words, CP reflects

how well the turbine utilizes the potential of wind energy to produce useful power. By understanding these two coefficients well, researchers can evaluate turbine performance more accurately under different operating conditions [34]. The equation is shown in Equation 5 [33].

$$Cp = \frac{P}{(1/2)\rho V^3 A} \quad (6)$$

In this formula, A is the cross-sectional area, P represents the power generated, v describes radius, and ρ is the air density. At the same time, v also refers to the turbine itself. Power (P) can be determined by multiplying the torque value by the rotor angular velocity (ω), as stated in Equation 7 [35].

$$P = Q.\omega \quad (7)$$

where Q is the torque and ω is the rotor's angular velocity. The torque (Q) is obtained from the calculation of Equations 6 and 7 [35].

$$C_Q = \frac{Q}{\frac{1}{2}\rho r A v^2} \quad (8)$$

$$Q = C_Q.\frac{1}{2}\rho r A v^2 \quad (9)$$

This equation defines (Cq) as the torque coefficient, while (ρ) describes the air density. In addition, (A) is the associated cross-sectional area (r) represents the radius, and (v) refers to the input rate applied in the context of this analysis. The blade's geometry parameter is chosen to evaluate, and it is crucial to determine if the turbine functions at a consistent or fluctuating rotational speed. The blade's geometry necessitates a streamlined design for higher tip speed ratios. Conversely, wind turbines with low tip speed ratios operate oppositely. A thinner and shorter spoon is necessary. Wind turbines often do not consistently run at the ideal tip speed ratio; instead, they adjust their tip speed ratio based on varying wind speeds [33].

3. *Results* and *discussion*

On rotors with a radius of 1.8 m and wind speeds of 2 m/s, 3 m/s, 4 m/s, 5 m/s and 6 m/s, as presented in Table 1. These data are used for numerical analysis to obtain analytical and simulation data for torque and power calculations from the wind turbine. Table 3 presents the simulated numerical computations on different configurations of wind turbine blades.

Table 3. Numerical results from CFD simulations on different types of wind turbine blade variations

Variation		w [rad/s]	Torque [Nm]	Power [W]
Blade	Velocity [m/s]			
BASE	2	15.5	3.72	57.57
	3	15.5	5.27	81.69
	4	15.5	6.09	94.41
	5	15.5	14.24	220.62
	6	15.5	23.13	358.36
SSHAWT 1	2	15.5	3.73	57.78
	3	15.5	5.32	82.37
	4	15.5	6.12	94.76
	5	15.5	14.30	221.48
	6	15.5	23.23	359.94
SSHAWT 2	2	15.5	3.77	58.38
	3	15.5	5.39	83.50
	4	15.5	6.15	95.25
	5	15.5	14.36	222.46
	6	15.5	23.26	360.42
SSHAWT 3	2	15.5	3.77	58.42
	3	15.5	5.41	83.74

4	15.5	6.16	95.46
5	15.5	14.37	222.57
6	15.5	23.38	362.25

These results show three HAWT wind turbine modifications to SSHAWT (Small-Scale Horizontal Axis Wind Turbine). After the simulation, several parameters, such as torque, show the results. The results showed that the more dimples used, the higher the torque and power generated. The less effective dimples become slight differences but can improve performance. From the trends seen in Table 3,

Fig shows an increase. Compared to the base blade artificial with SSHAWT 3, the rise in the number of turbine blades is in addition to optimizing the wind turbine blade development with the addition of dimples. Still, it is also influenced by wind speed, with an average increase of approximately 5.2%.

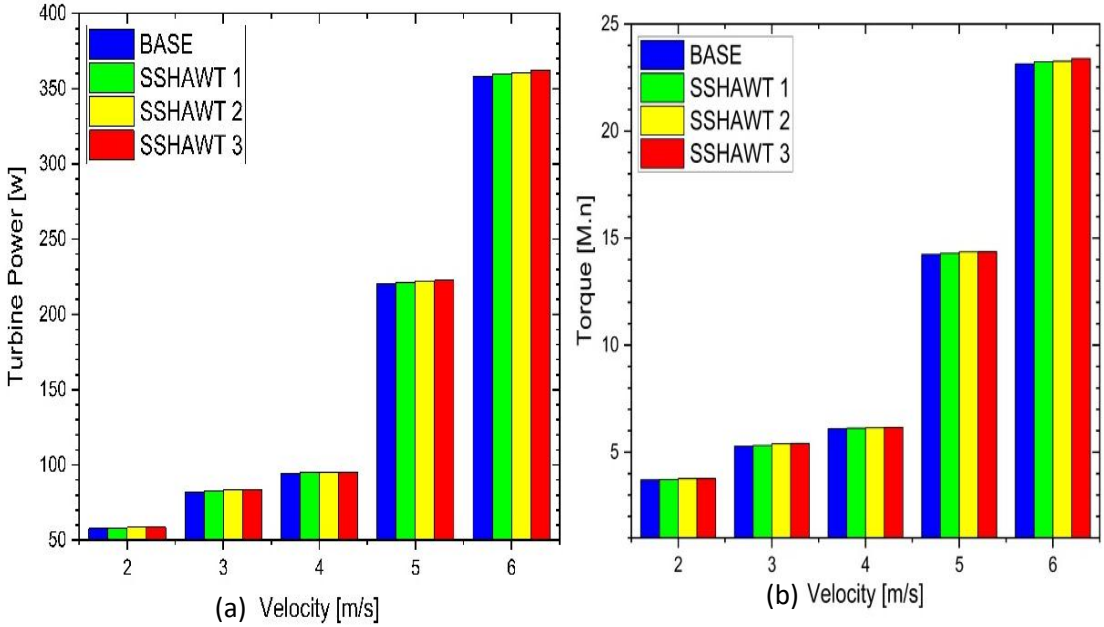

Fig 4. The result (a) Turbine Torque (M.n) (b) Turbine Power (*w*)

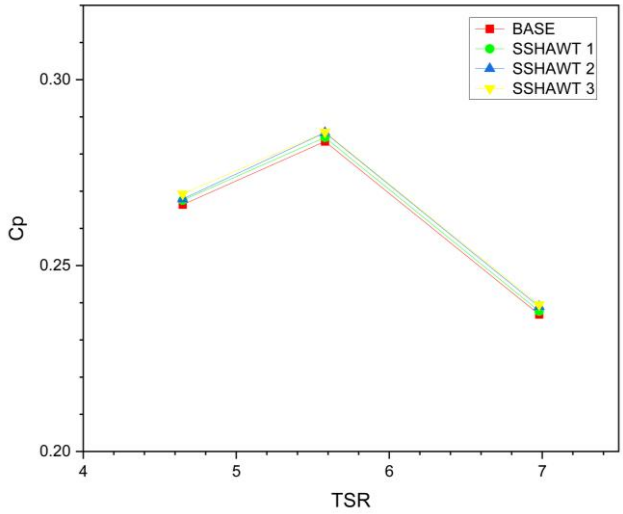

Fig 5. The result of performance curve variation of SSHAWTs (Cp vs TSR)

Figure 5 provides a comprehensive overview of the relationship between the power coefficient and the tip speed ratio in the context of different wind speed variations. Data analysis shows that the power coefficient ranges from 0.23 to 0.28 when the wind speed fluctuates between 3 m/s and 6 m/s. This reflects the turbine's ability to efficiently convert wind kinetic energy into mechanical energy within the speed range. In particular, the SSHAWT 3 turbine shows a significant power coefficient value of 0.285 at a nominal wind speed of 3 m/s. This figure shows good performance and the turbine's potential to generate power at lower wind conditions. The analysis also identified that this system's optimal tip speed ratio is around 5.58. This ratio is an important indicator, as it indicates the point at which maximum efficiency

is achieved in wind energy conversion. With an optimal tip speed ratio, the turbine can operate under conditions that support maximum energy extraction from the available wind, contributing to reduced operating costs and increased power output. These findings contribute to the fundamental understanding of small-scale wind turbine performance and have practical implications for future turbine design and development. By leveraging these insights, engineers and researchers can design more efficient and effective turbines utilizing available wind resources and improve the sustainability of renewable energy in various application.

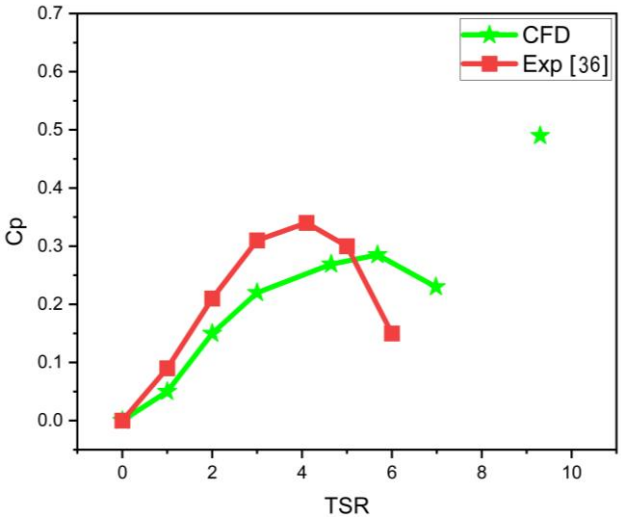

Fig 6. Comparison of current SSHAWT power coefficients with experimental and numerical data.

Figure 6 presents the validation of numerical results for the SSHAWT by comparing the CFD outcomes with empirical and numerical data from R. Anant Kishore and S. Priya [36], who studied small wind energy portable turbines (SWEPT). The comparison is based on the power coefficient (Cp) across seven tip speed ratios (TSRs) ranging from 1 to 6. The analysis shows a strong agreement between the Computational Fluid Dynamics (CFD) simulation results and the experimental data obtained, reflected in all Turbine Speed Ratio (TSR) values. This finding indicates that the CFD model can reliably represent the operational conditions of the wind turbine and provides a strong validation of the simulation approach applied in this study, with the CFD simulation accurately reproducing the experimental Cp peak at $\lambda = 6$. Despite some deviations, the overall trends in the analysis are consistent with the experimental data, and the observed errors are relatively constant. These discrepancies are mainly attributed to the inherent limitations of the model, especially regarding additional dimples on the suction side of the blades, which resulted from unexpected performance gains.

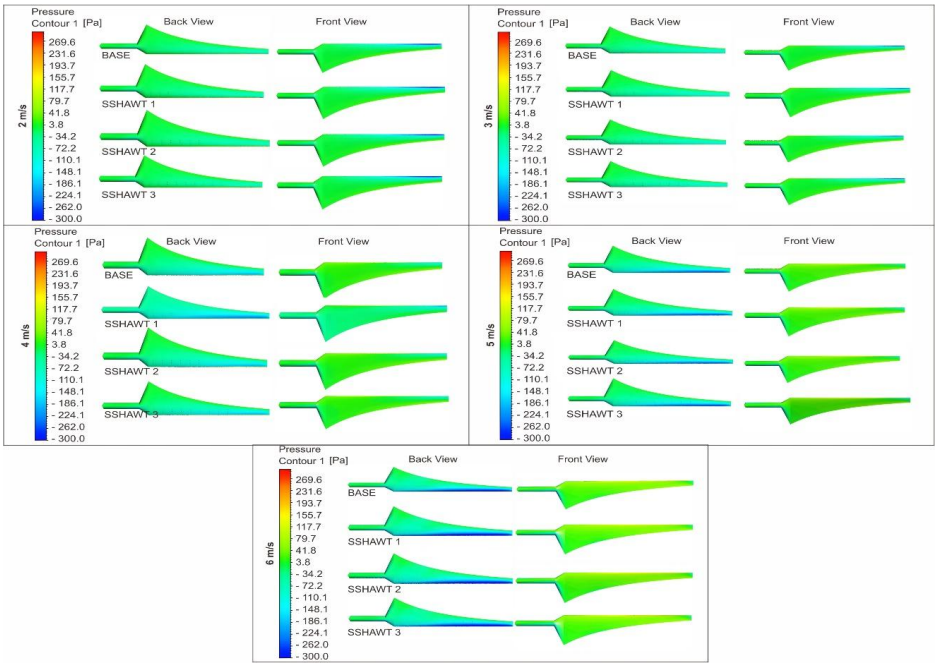

Fig. 7. Pressure contour CFD modeling result

Fig.7 shows the pressure contour of the wind turbine blades on the front (suction side) and back (pressure side). The picture shows that the back has a specific green colour compared to the front, which still has a blue colour. The legend indicates that green has a more excellent pressure value of about 269 Pa while blue has a small value of about -300 Pa. From this colour gradient, the back of the wind turbine blade has a higher or greater pressure than the back. This pressure difference causes a force to rotate the wind turbine blade on its rotary axis due to the torque generated.

The different results occur due to modifications of the number of bumps present on the front of relating to the turbine's blade or the suction side. Adding dimples on the suction side will affect the pressure distribution on the part. The data in Fig. 4 shows that adding dimples will increase the torque and turbine power value. At the same time, torque itself is a force multiplied by distance. A difference in pressure on the pressure side or the back with the suction side or the front makes the force wind turbine blade. This shows that the pressure difference between the pressurized side and the suction side will increase with the addition of dimples. See more details in Fig. 4 and Table 2. The dimples to the wind turbine blade make the suction area or area with a smaller pressure value spacious with constant pressure side conditions in each dimple's addition. The pressure difference becomes higher because the torque increases. Adding dimples will make the suction area larger, especially in dimples close to the tip area. On the SSHAWT 3 turbine, it is getting closer to the tip so that the suction side pressure on the front becomes wider in area.

Fig. 8 shows the velocity flow contour image taken on the wind turbine blade section at a distance with dimples on the second, fifth, and eighth sections. The contour of this velocity indicates the fluid velocity distribution passing through the turbine. At the top of the airfoil or in the image, it is on the top. Then, a greener contour, a greener contour is at the bottom of the airfoil with a bluer colour. This indicates that the airfoil area at the top has a higher fluid flow speed than the bottom. Then, the farther the distance of the contour capture speed, the higher and higher the maximum speed. For all variations in the second section, the maximum speed reaches 6 m/s, and then the maximum speed reaches 12 for the fifth section. m/s, and for the eighth section, the maximum speed reaches 25 m/s.

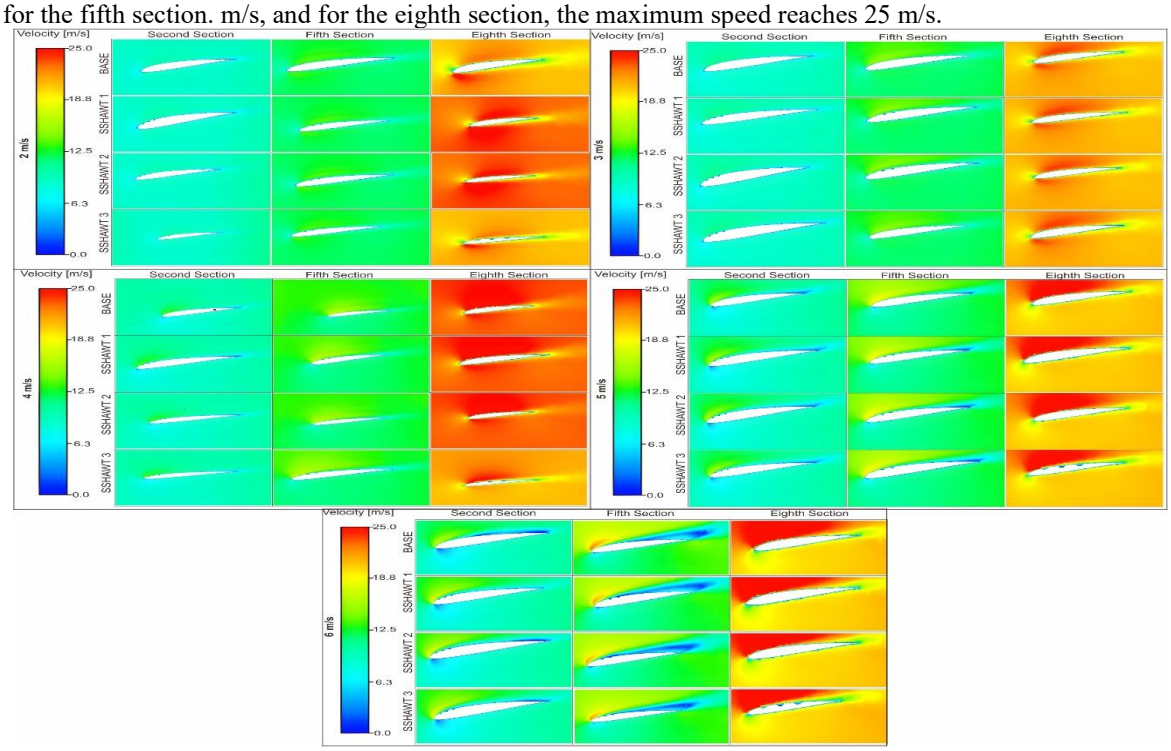

Fig. 8. Velocity flow contour CFD modeling result

Fig. 8 also shows the influence of the addition dimples on the speed contours at each distance of the sample taken. In the distance of the second section, the speed contours of the base and SSHAWT 1, 2, and 3 turbines have the exact visualization, and the difference is that the speed increases when the fluid passes through the dimples. The increase in speed in the area contained in the dimples will lower the pressure that will enlarge the suction area or low pressure so that the presence of dimples will increase the speed in the dimples area. So, the suction side becomes wider, resulting in a decrease in pressure on the dimple area. The visual Fig. 9 concluded that the turbine blades of SSHAWT 3 are the best in extracting wind flow. The more dimples added, the better it will be at the wind suction. In construction, the dimples can section the wind into the dimple hole so that the dimples can help drive the wind turbine blades faster. On the streamline, the flow line hits more of the suction side of the wind turbine blade and more evenly flows across the side of the wind turbine blade. Compared to the SSHAWT 1 and SSHAWT 2 turbines, the SSHAWT 3 turbine's wind turbine blades are likewise becoming greener.

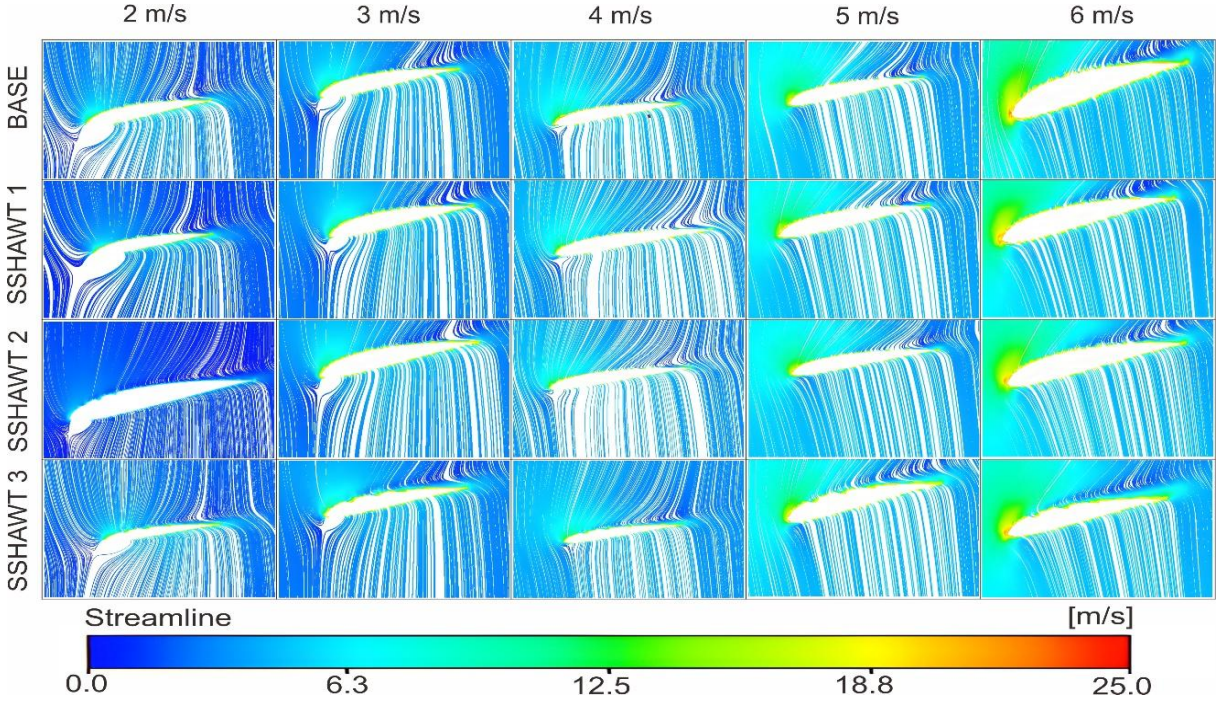

Fig. 9. Streamline velocity distribution CFD modeling result.

4. *Conclusion*

This study proposes an approach that Computational Fluid Dynamics (CFD) to develop a Structure-Fluid Dynamics Interaction (FSI) model. The focus of this model is on a small-scale wind turbine blade positioned on a horizontal axis, allowing a comprehensive analysis of the mechanical behavior and aerodynamic response of the blade under operational conditions with one-way coupling, The FSI model is used to simulate SSHAWT blades through FSI modeling and is confirmed through benchmark computer testing. From this study, the following findings can be made, The aerodynamic component of the FSI model, which depends on CFD, is validated by obtaining a reasonable agreement with a maximum angular velocity of 15.5 rad/s when compared to the FAST code. The optimal blade optimization over small scale turbines of wind power optimization is demonstrated by the SSHAWT 3 turbine, which produced the highest power exode of 362.25 w at a wind speed of 6 m/s.

Studies for the future that can be done are by varying dimples in areas other than the suction side and the number of dimples that can be added to small-scale horizontal wind turbine blades, as well as trying to prototype so that detailed analysis of CFD can be a viable application for determining the strength and performance of small-scale horizontal winds.

Declaration of interest: The authors declare no conflicts of interest

Reference

[1] R. S. Jackson and R. Amano, "Experimental Study and Simulation of a Small-Scale Horizontal-Axis Wind Turbine," *J. Energy Resour. Technol. Trans. ASME*, vol. 139, no. 5, pp. 1–19, 2017.

[2] Ismail, E. A. Pane, G. Haryanto, T. Okviyanto, and R. A. Rahman, "A better approach for modified bach-type savonius turbine optimization," *Int. Rev. Aerosp. Eng.*, vol. 14, no. 3, pp. 159–165, 2021.

[3] A. R. Ali, M. Z. Akhter, and F. K. Omar, "Performance enhancement of a small-scale wind turbine featuring morphed trailing edge," *Sustain. Energy Technol. Assessments*, vol. 46, no. April, p. 101229, 2021.

[4] E. Maroha, "Aerodynamic and Modal Analyses of Small Scale Horizontal Axis Wind Turbine with Various Numbers of Blade Design," 2016.

[5] F. Butt *et al.*, "Effect of the shape of flapping airfoils on aerodynamic forces," *Heliyon*, vol. 10, no. 8, 2024.

[6] P. Freere, M. Sacher, J. Derricott, and B. Hanson, "A low cost wind turbine and blade performance," *Wind Eng.*, vol. 34, no. 3, pp. 289–302, 2010.

[7] R. K. Singh and M. R. Ahmed, "Blade design and performance testing of a small wind turbine rotor for low wind speed applications," *Renew. Energy*, vol. 50, pp. 812–819, 2013.

[8] M. Sessarego, J. Feng, N. Ramos-García, and S. G. Horcas, "Design optimization of a curved wind turbine blade using neural networks and an aero-elastic vortex method under turbulent inflow," *Renew. Energy*, vol. 146, pp. 1524–1535, 2020.

[9] J. W. Wang, H. Xu, and N. Ma, "Investigation on self-adaptive vibration suppression for cantilever Euler beam

with interior inlaid fluid under principal resonance excitation," *Zhendong yu Chongji/Journal Vib. Shock*, vol. 30, no. 8, pp. 41–44, 2011.
[10] Ismail, Rinawati, and Imam Muzaki, "Investigation of Vertical Axis Wind Turbine Performance with Savonius Rotor on Air Ejector Dimensions using Computational Fluid Dynamics," *CFD Lett.*, vol. 16, no. 5, pp. 121–134, Jan. 2024.
[11] Ismail, J. John, E. A. Pane, R. Maulana, R. A. Rahman, and A. Suwandi, "Experimental evaluation for the feasibility of test chamber in the open-loop wind tunnel," *WSEAS Trans. Fluid Mech.*, vol. 16, pp. 120–126, 2021.
[12] R. Gukendran, M. Sambathkumar, C. Sabari, C. R. Ranjith Raj, and V. Ranjeeth Kumar, "Structural analysis of composite wind turbine blade using ANSYS," *Mater. Today Proc.*, no. xxxx, 2021.
[13] X. Li and J. Xu, "Overall design optimization of dedicated outboard airfoils for horizontal axis wind turbine blades," no. November 2017, pp. 1–18, 2018.
[14] M. G. Mourad, T. A. Mekhail, I. Shahin, and O. E. Abdellatif, "Effect of winglet geometry on horizontal axis wind turbine performance," no. December 2019, pp. 1–19, 2020.
[15] M. G. Khalafallah and A. M. Ahmed, "The effect of using winglets to enhance the performance of swept blades of a horizontal axis wind turbine," vol. 11, no. 9, pp. 1–10, 2019.
[16] V. D'Alessandro, G. Clementi, L. Giammichele, and R. Ricci, "Assessment of the dimples as passive boundary layer control technique for laminar airfoils operating at wind turbine blades root region typical Reynolds numbers," *Energy*, vol. 170, pp. 102–111, 2019.
[17] H. Sedighi, P. Akbarzadeh, and A. Salavatipour, "Aerodynamic performance enhancement of horizontal axis wind turbines by dimples on blades : Numerical investigation," *Energy*, vol. 195, p. 117056, 2020.
[18] V. Madhanraj, E. H. Reddy, S. S. Basha, K. G. K. Murthy, and G. B. Chandra, "Investigation and Analysis of The Performance Characteristics of Horizontal Axis Wind Turbine Blade with Dimple By Using CFD," vol. 12, no. 7, pp. 47–52, 2021.
[19] F. Azlan, M. K. Tan, B. T. Tan, and M.-Z. P. Ismadi, "Passive Flow-Field Control Using Dimples for Performance Enhancement of Horizontal Axis Wind Turbine," *SSRN Electron. J.*, pp. 1–30, 2022.
[20] P. W. Bearman and J. K. Harvey, "Golf Ball Aerodynamics," *Aeronaut. Q.*, vol. 27, no. 2, pp. 112–122, May 1976.
[21] N. Beratlis, E. Balaras, and K. Squires, "On the origin of the drag force on dimpled spheres," *J. Fluid Mech.*, vol. 879, pp. 147–167, 2019.
[22] S. Rehman, M. Mahbub Alam, L. M. Alhems, and M. Mujahid Rafique, "Horizontal AxisWind Turbine Blade Design Methodologies for Efficiency Enhancement A Review," *Energies*, vol. 11, no. 3, 2018.
[23] S. J. Miley, "Catalog of low-Reynolds-number airfoil data for wind-turbine applications," Feb. 1982.
[24] P. Arumugam, V. Ramalingam, and K. Bhaganagar, "A pathway towards sustainable development of small capacity horizontal axis wind turbines – Identification of influencing design parameters & their role on performance analysis," *Sustain. Energy Technol. Assessments*, vol. 44, no. June 2020, p. 101019, 2021.
[25] Y. Xie, D. Shi, and Z. Shen, "Experimental and numerical investigation of heat transfer and friction performance for turbine blade tip cap with combined pin-fin-dimple/protrusion structure," *Int. J. Heat Mass Transf.*, vol. 104, pp. 1120–1134, 2017.
[26] A. Suresh and S. Rajakumar, "Design of small horizontal axis wind turbine for low wind speed rural applications," *Mater. Today Proc.*, vol. 23, no. xxxx, pp. 16–22, 2019.
[27] "Airfoil Tools." [Online]. Available: http://airfoiltools.com/index.
[28] L. Wang, R. Quant, and A. Kolios, "Fluid structure interaction modelling of horizontal-axis wind turbine blades based on CFD and FEA," *J. Wind Eng. Ind. Aerodyn.*, vol. 158, pp. 11–25, 2016.
[29] F. R. Menter, "Two-equation eddy-viscosity turbulence models for engineering applications," *https://doi.org/10.2514/3.12149*, vol. 32, no. 8, pp. 1598–1605, May 2012.
[30] Ismail *et al.*, "Computational fluid dynamics simulation of the turbulence models in the tested section on wind tunnel," *Ain Shams Eng. J.*, vol. 11, no. 4, pp. 1201–1209, 2020.
[31] M. M. Yelmule and V. S. J. EswaraRao Anjuri, "CFD predictions of NREL phase VI rotor experiments in NASA/AMES wind tunnel," *Int. J. Renew. Energy Res.*, vol. 3, no. 2, pp. 261–269, 2013.
[32] P. Bourdin and J. D. Wilson, "Windbreak aerodynamics: Is computational fluid dynamics reliable?," *Boundary-Layer Meteorol.*, vol. 126, no. 2, pp. 181–208, 2008.
[33] M. M. Hasan, "Design and Performance Analysis of Small Scale Horizontal Axis Wind Turbine for Nano Grid Application," 2017.
[34] F. Zhu, L. Ding, B. Huang, M. Bao, and J.-T. Liu, "Blade design and optimization of a horizontal axis tidal turbine," *Ocean Eng.*, vol. 195, p. 106652, Jan. 2020.
[35] E. H. Lysen, *Introduction to Wind Energy*. .
[36] R. A. Kishore, T. Coudron, and S. Priya, "Small-scale wind energy portable turbine (SWEPT)," *J. Wind Eng. Ind. Aerodyn.*, vol. 116, pp. 21–31, 2013.